

RSC Advances



This is an *Accepted Manuscript*, which has been through the Royal Society of Chemistry peer review process and has been accepted for publication.

Accepted Manuscripts are published online shortly after acceptance, before technical editing, formatting and proof reading. Using this free service, authors can make their results available to the community, in citable form, before we publish the edited article. This *Accepted Manuscript* will be replaced by the edited, formatted and paginated article as soon as this is available.

You can find more information about *Accepted Manuscripts* in the [Information for Authors](#).

Please note that technical editing may introduce minor changes to the text and/or graphics, which may alter content. The journal's standard [Terms & Conditions](#) and the [Ethical guidelines](#) still apply. In no event shall the Royal Society of Chemistry be held responsible for any errors or omissions in this *Accepted Manuscript* or any consequences arising from the use of any information it contains.

The preparation of Fe₂O₃ nanoparticles by liquid phase-based ultrasonic-assisted method and its application as enzyme-free sensor for the detection of H₂O₂

Chen Hao^{a,*}, Feng Feng^a, Xiaohong Wang^{a,*}, Min Zhou^a, Yutao Zhao^b, Cunwang Ge^c, Kun Wang^a

^a School of Chemistry and Chemical Engineering, Jiangsu University, Zhenjiang, Jiangsu 212013, China

^b School of Material Science & Engineering, Jiangsu University, Zhenjiang, Jiangsu 212013, China

^c School of Chemistry and Chemical Engineering, Nantong University, Nantong, Jiangsu 226019, China

Abstract: Iron oxide nanoparticles with high electrocatalytic activity for hydrogen peroxide was developed by liquid phase-based ultrasonic-assisted method using sodium lignosulphonate as surfactant. The influence of the different preparation conditions including additions of sodium lignosulphonate (SLS) and calcining temperatures was investigated by X-ray diffraction (XRD), scanning electron microscopy (SEM), transmission electron microscope (TEM), and Brunauer- Emmett-Teller (BET) specific surface area. Then, the as-prepared Fe₂O₃ with graphene (G) was further fixed on the surface of glassy carbon electrode (GCE) using chitosan (CS) as a crosslinking agent. The electrochemical properties of the prepared G-Fe₂O₃-NPS-CS/GCE sensor were estimated by cyclic voltammetry and chronoamperometry. Finally, the G-Fe₂O₃-NPS-CS/GCE (1.0g SLS, calcined 400°C) sensor showed an excellent electrocatalytic activity towards hydrogen peroxide, which displayed high sensitivity (385.59 $\mu\text{A mM}^{-1} \text{cm}^{-2}$), wide detection range (0.5- 7800 μM), low detection limit (0.5 μM) and a fast response time less than 2s. Furthermore, the sensor also exhibited good anti-interference for ascorbic acid and uric acid, excellent repeatability and long-term stability. These results indicated that the G-Fe₂O₃-NPS-CS/GCE (1.0g SLS, calcined 400°C) sensor held great potential for the detection of hydrogen peroxide.

26

27 *Corresponding author. Tel.: +86 511 88791800; fax: +86 511 88791800.

28 E-mail addresses: chhao@ujs.edu.cn (C. Hao); xhwang@ujs.edu.cn (X.H. Wang).

29

30 **Keywords:** Iron oxide; Liquid phase; Enzyme-free sensor; Electrochemical properties;
31 Hydrogen peroxide.

32 **Introduction**

33 Nanomaterials has become one of the most active research orientations in the areas of
34 physics, chemistry, and engineering since 1990, due to the small particle size, large specific
35 surface area, high surface energy and unique surface effect, small-size effect, and
36 macroscopical quanta tunnel effect, etc.¹⁻⁴ In the past several decades, various types of
37 nanomaterials such as Au, Ag, TiO₂, SiO₂, and ZnO etc. have been widely applied as
38 photocatalyst, functional ceramics, sensor, solar cell and biology functional material.⁵⁻⁹ Among
39 the various kinds of nanomaterials, iron oxide as an important oxide has been studied for a wide
40 range of applications because it is environmentally friendly, non-toxic, heat-resistant, and
41 corrosion-resistant material.^{10,11} At the same time, because of the low density, large surface,
42 high stability, and remarkable sensitivity of the conductivity to temperature, humidity and
43 concentration, the Fe₂O₃ semiconductor shows a broad and good prospect for application in the
44 field of sensing materials.

45 On the other hand, the reliable and rapid determination of hydrogen peroxide (H₂O₂) is of
46 great importance in biology and chemistry fields because it is not only used as an important
47 oxidizing agent in food and chemical industries, but also widely used as a mediator in food,
48 pharmaceutical, clinical, industrial and environmental analysis.¹²⁻¹⁵ Many techniques have been
49 successfully used for the detection of H₂O₂, such as titrimetry, spectrophotometry, fluorescence,
50 chemiluminescence and electrochemistry. Compared with other detection methods,
51 electrochemistry has attracted more and more interest of researchers, due to the convenience,
52 high sensitivity, and excellent precision of the technique.¹⁶⁻¹⁸ Some electrochemical sensors

53 with a high sensitivity and specificity for detection of H_2O_2 , such as
54 NF/CAT/MWCNTs-COOH/Cys-AuNPs/GC, CAT/MgO-NPs/CPE, GC/MWCNT-NiO/CAT and
55 GC/MWCNTs/[bmim][PF₆]/CAT have been successfully developed.¹⁹⁻²² Most of the above
56 mentioned electrochemical sensors were constructed based on enzymes or proteins.
57 Enzyme-modified electrochemical sensors can achieve high sensitivity and excellent selectivity,
58 however, there are many defects of enzyme-based electrochemical sensors, such as instability,
59 limited lifetime, high cost and complicated modification procedure. Its activity, meanwhile, can
60 be easily affected by temperature, pH value and oxygen.²³⁻²⁷ In comparison with the
61 enzyme-modified sensors, the enzyme-free sensor's research becomes very meaningful due to
62 their long lifetime, high environmental suitability and high durability.

63 Iron oxide has been a good choice to be used as substrate for enzyme-free sensors due to
64 its good chemical stability, low-cost and narrow band gap (-2.1 eV).²⁸ It is well-known that the
65 excellent performance of the material depends not only on the characteristic of the material
66 itself, but also on the size, crystallinity and morphology of the material particle.²⁹ There are
67 always some problems like agglomeration of particles, large particle size, etc. exist during the
68 preparation of iron oxide. Therefore, control of the size and morphology of Fe_2O_3 has attracted
69 more and more attention of researchers. Up to now, some Fe_2O_3 particles with excellent
70 properties have been synthesized through various methods with the assistance of different
71 surfactants.³⁰⁻³²

72 In this paper, a technically simple and cost-effective ultrasonic method for synthesizing
73 Fe_2O_3 nanoparticle in the presence of SLS has been developed in order to obtain the desired
74 sensor materials. Then, the as-prepared Fe_2O_3 nanoparticle and graphene, were immobilized
75 onto the GCE surface by chitosan. Cyclic Voltammetry and Chronoamperometry are used to

76 determine the electrochemical properties of the sensor. The resulting sensor exhibited high
77 sensitivity, a wide linear range and a lower detection limit for hydrogen peroxide.

78 **Experimental**

79 **Materials**

80 Ferric chloride, carbamide, potassium permanganate, flake graphite, hydrazine hydrate and
81 hydrogen peroxide were purchased from Sinopharm Chemical Reagent Co., Ltd. (Shanghai,
82 China). Concentrated hydrochloric acid (36-38%, m/m) and concentrated sulfuric acid (98%,
83 m/m) were purchased from Yangzhou Hubao Chemical Reagent Co., Ltd. (Yangzhou, China).
84 SLS of industrial grade was bought from Fei Wong Xinyi Chemical Co., Ltd (Xuzhou, China).
85 All other reagents were of analytical grade and used without further purification. 0.2% (m/m)
86 chitosan solution was prepared by addition of chitosan in 1% (m/m) acetic acid solution. 0.1 M
87 of pH=7.4 phosphate buffer solution (PBS) was adjusted by 0.1 M K_2HPO_4 and KH_2PO_4 . All
88 as-prepared solution were stored at 4°C when not in use.

89 **Preparation of Fe_2O_3 nanoparticle and graphene**

90 Fe_2O_3 nanoparticles were synthesized by liquid phase-based ultrasonic-assisted method in the
91 following way: 4.06g $FeCl_3 \cdot 6H_2O$ was dissolved in 250mL double-distilled water with certain
92 amount of SLS and the mixed solution was sonicated in the water bath of 85°C until a relatively
93 steady solution system was formed. Then a 50ml solution of 1.2M $(NH_2)_2CO$ was added to the
94 system drop by drop, and the reaction system was refluxed for 4h. The resultant solids were
95 collected by filtration and repeated washing. After that, the solid was dried in oven at 60°C, and
96 then calcined at 300°C, 400°C, 500°C and 600°C in furnace for 2h, respectively. The added
97 amounts of SLS were 0, 0.5, 1.0, 1.5, 2.0g, respectively.

98 Graphite oxide was prepared using flake graphite by a modified Hummer's method³³. First,
99 graphite powder was oxidized by $KMnO_4$ / $NaNO_3$ and H_2SO_4 , and the Graphite oxide was

100 exfoliated into graphene oxide by a KQ-250 ultrasonic reactor (Kunshan, China, P=250W,
101 $f=40\text{kHz}$). Subsequently, the unexfoliated graphite oxide is separated by centrifugation at
102 2000RPM for 10min. Finally, the obtained back suspension of graphene oxide is reduced into
103 graphene using hydrazine. The graphener was washed for several times and stored at 4°C .

104 **Preparation of the modified electrodes**

105 The preparation of the G- Fe_2O_3 -NPS-CS/GCE modified electrode is described as follows:

106 Prior to use, the bare glassy carbon electrode (GCE, 4mm in diameter) was carefully polished to
107 a mirrorlike surface with emery paper and $1.0\mu\text{m}$, $0.5\mu\text{m}$ alumina slurry, respectively. Then the
108 polished electrode was rinsed ultrasonically in acetone, absolute ethanol, deionized water for
109 3min, respectively. The electrode was activated using repeatedly cyclic voltammetry scanned
110 from -1.0 to 1.0V at $50\text{mV}\cdot\text{s}^{-1}$ in $1.0\text{M H}_2\text{SO}_4$ until a stable voltammogram was obtained. To
111 prepare the modified composite, 3mg of Fe_2O_3 and 2mg of graphene are mixed in 0.2% (m/m)
112 chitosan solution, and this mixture was sonicated for 30min to acquire a homogeneous and
113 well-dispersed black suspension. Whereafter, $3\mu\text{L}$ of the suspension was smeared evenly onto
114 surface of the GCE electrode. In order to obtain a more uniform modified films , the
115 as-prepared electrode was slow dried at 4°C . The obtained G- Fe_2O_3 -NPS-CS/GCE modified
116 electrodes was stored at 4°C . Meanwhile, the Fe_2O_3 -NPS -CS/GCE modified electrode was also
117 prepared. Iron oxide and graphene easily fall off from the surface of electrode without the
118 adhesive force of chitosan (CS) for the G- Fe_2O_3 -NPS/GCE modified electrode. Therefore, the
119 G- Fe_2O_3 -NPS/GCE has not been discussed in this work. The G- Fe_2O_3 -NPS-CS/GCE (1.0g SLS ,
120 calcined 400°C) are denoted as G- Fe_2O_3 -CS/GCE-1-400.

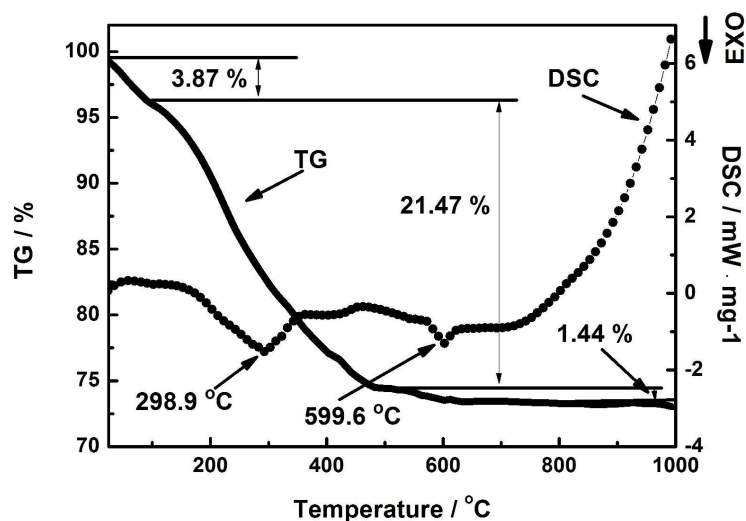
121 **Characterizations**

122 Thermogravimetric/differential scanning calorimetry (TG/DSC) analysis was performed

123 using a integrated thermal analyzer (STA449C, NETZSCH) under a nitrogen atmosphere with a
124 heating rate of $5^{\circ}\text{C} \cdot \text{min}^{-1}$ from 25°C to 1000°C . FT-IR spectra of the powders (as pellets in KBr)
125 were recorded using Fourier transform infrared spectroscopy (FT-IR, Nicolet,
126 AVATAR-370MCT) in the range of $4000\text{--}400 \text{ cm}^{-1}$. The XRD patterns of the Fe_2O_3
127 nanoparticles were recorded using a Bruker D8 Advance X-ray diffractometer at a voltage of 40
128 kV and current of 40 mA with Cu $K\alpha$ radiation ($\lambda = 0.15406 \text{ nm}$). The specific surface area and
129 pore size data were obtained by Surface area and porosity analyzer (NOVA- 2000e). The
130 morphology of the nanoparticles was examined with the Field Emission Scanning Electron
131 Microscope (FE-SEM, S4800, HI-9140-0006). All electrochemical experiments were
132 performed by a CHI 660C electrochemical workstation (Chen Hua Instrumental Corporation,
133 Shanghai, China). A conventional three-electrode system (including the modified GCE as the
134 working electrode, a platinum foil as the counter electrode and a saturated calomel electrode
135 (SCE) as the reference) was employed to test electrochemical property of modified electrode.

136 **Results and discussion**

137 TG–DSC measurement was performed to investigate the decomposition behavior and the
138 phase transition temperatures of the as-synthesized precursor (FeOOH) containing 1.0g SLS.
139 The results are exhibited in Fig. 1.



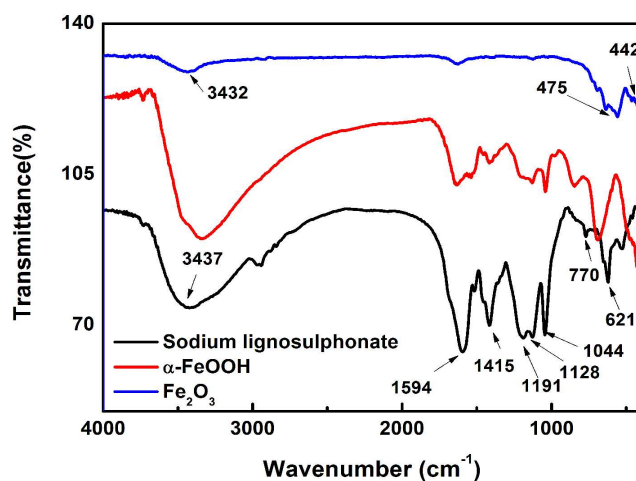
140
141

Fig. 1 DSC-TGA curve for α -FeOOH precursor containing SLS

142 The curve of TG shows that the first weight loss was about 3.87% in temperature range of
143 25°C to 100°C, which is attributed to the dehydration of the physical adsorption on the sample
144 surface. The relatively large weight loss of 21.47% occurred from 100°C to 480°C, and the
145 corresponding exothermic peak was observed at 298.9 °C in the DSC curve. This is because of
146 the decomposition of the α -FeOOH³⁴ and SLS at high temperature. The third mass loss of
147 1.44% from 480°C to 820°C is attributed to the continued decomposition of SLS surrounded by
148 Fe₂O₃. No obvious weight loss over 820°C. Subsequently, the DSC curve shows that the small
149 exothermic peak at 599.6°C is mainly due to the phase transformation from γ -Fe₂O₃ to
150 α -Fe₂O₃.³⁵

151 The FT-IR spectra as an important analytical technique was used to evaluate the structural
152 changes of the different samples shown in Fig. 2. It can be found that there are large numbers of
153 functional groups of SLS among the as-prepared α -FeOOH containing 1.0g SLS. The results
154 indicate that the SLS has been successfully embedded in the α -FeOOH precursor. Accompanied
155 by the thermal decomposition of α -FeOOH precursor into Fe₂O₃, the characteristic peaks of
156 SLS almost all disappeared due to the volatilization and decomposition of SLS. The two

157 obvious absorption peaks at 475cm^{-1} and 442cm^{-1} are attributed to the vibration of the $\text{Fe}^{3+}\text{-O}^{2-}$.

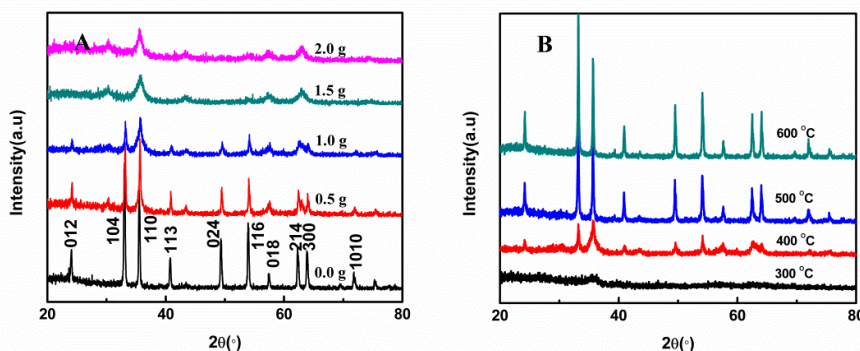


158

159

Fig.2 FT-IR spectra of sodium lignosulphonate, $\alpha\text{-FeOOH}$ and Fe_2O_3 .

160



161

162 Fig. 3 (A) XRD patterns of as-prepared Fe_2O_3 samples with different additions of SLS
163 calcined at 400°C . (B) XRD patterns of Fe_2O_3 samples prepared with 1.0g SLS calcined at
164 300°C , 400°C , 500°C and 600°C .

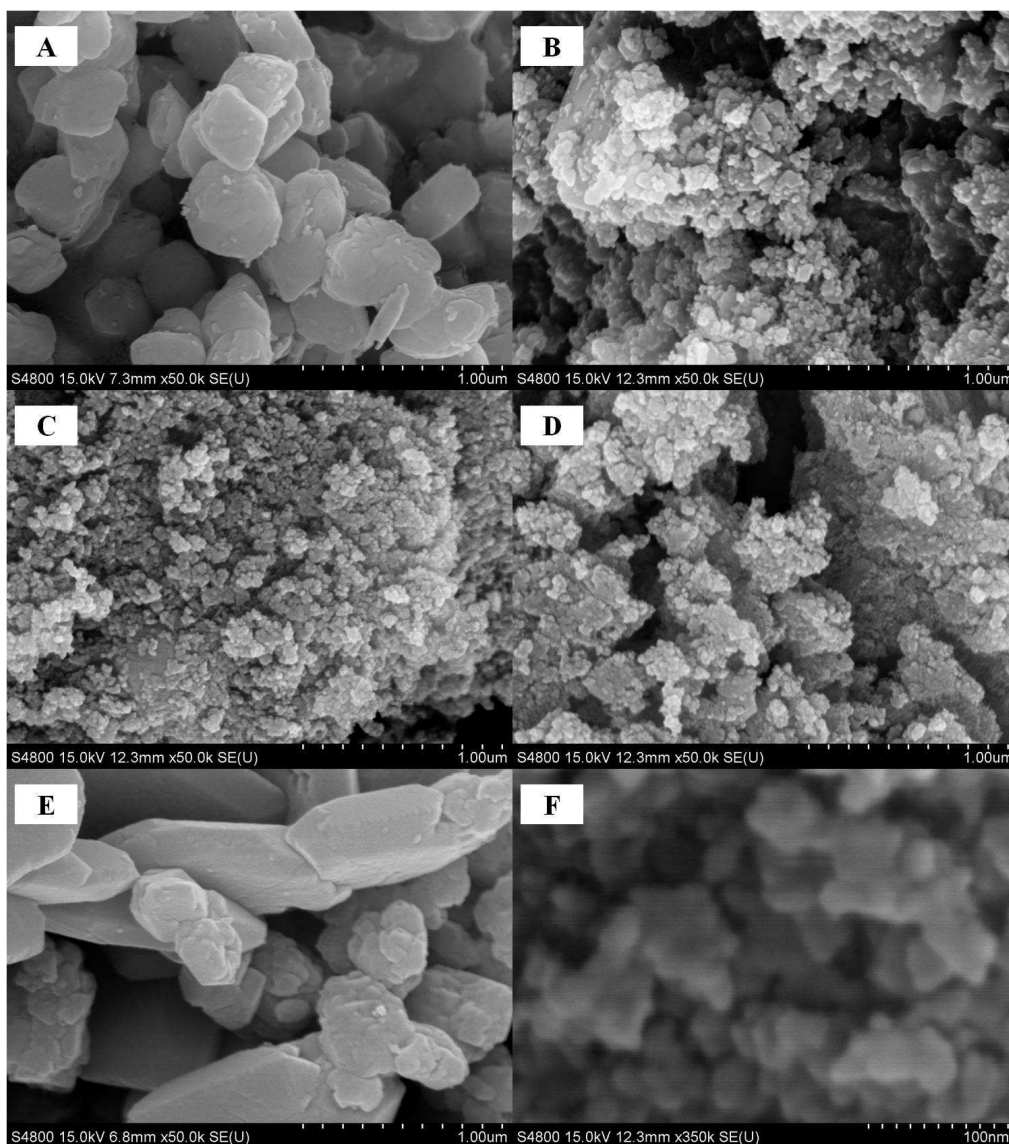
165 Fig. 3A shows the XRD patterns of the as-prepared samples with varied additions of SLS
166 calcined at 400°C . The curve with the narrowest and sharpest peaks in Fig. 3A indicates the best
167 crystallized Fe_2O_3 for the addition of no SLS. All XRD peaks at $2\theta = 24.1^\circ(012)$, $33.2^\circ(104)$,
168 $35.6^\circ(110)$, $40.9^\circ(113)$, $49.5^\circ(024)$, $54.1^\circ(116)$, $57.4^\circ(018)$, $62.5^\circ(214)$, $64.0^\circ(300)$ and
169 $72.0^\circ(1010)$ can be clearly indexed to the rhombohedral phase of hematite (JCPDF
170 No.33-0664). No characteristic peaks of any other impurities are detected. The diffraction peak
171 be gradually weakened at (012), (104), (113), (024), (214), (300) and (1010) with the

172 increasement of SLS. These characteristic peaks almost disappear for the addition of 2.0g SLS.
 173 Meanwhile, it is obvious to compare the JCPDF cards that we can find the transformation of
 174 Fe₂O₃ crystalline structure from the rhombohedral symmetry (JCPDS No. 33-0664) to
 175 Maghemite (JCPDS No. 39-1346) with the increasing SLS content. In addition, The influence
 176 of different calcination temperature was also discussed, as shown in Fig. 3B. The Fe₂O₃ samples
 177 calcined at 300°C showed wider and weaker diffraction peaks, and displayed poorer
 178 crystallization than the other Fe₂O₃ samples. As expected, the diffraction peaks' intensity of
 179 Fe₂O₃ constantly reinforced with an ever-increasing calcination temperature, accompanied with
 180 the gradual growth of Fe₂O₃ nanoparticles. γ -Fe₂O₃ was successfully transformed to α -Fe₂O₃
 181 with the increase in the annealing temperature. The average crystallite dimension (ACD) of all
 182 samples was estimated through using Scherrer formula, $D = 0.9\lambda/\beta\cos\theta$, where D is the average
 183 crystalline size, λ is the wavelength of Cu K α ($\lambda=0.15406$ nm), β is the full width at half
 184 maximum of the diffraction peaks, and θ is the Bragg's angle. the results of the computation are
 185 shown in Tab. 1.

186 Tab. 1 ACD and BET of different Fe₂O₃ samples.

SLS/g	T/°C	ACD/nm	BET/m ² ·g ⁻¹	SLS/g	T/°C	ACD/nm	BET/m ² ·g ⁻¹
0.0	400	32.03	8.208	2.0	400	9.26	46.311
0.5	400	26.78	27.430	1.0	300		76.196
1.0	400	21.86	81.319	1.0	500	32.13	21.367
1.5	400	10.06	71.912	1.0	600	36.21	11.709

187



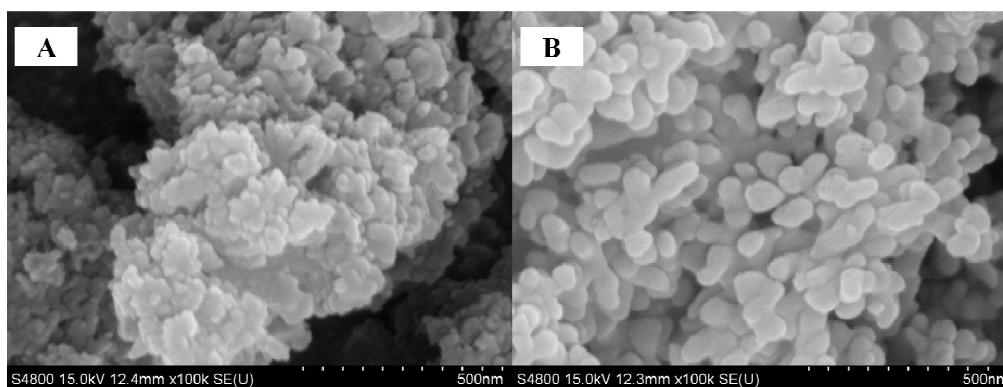
188

189

190 Fig. 4 SEM images of Fe₂O₃ samples with different additions of SLS calcined at 400 °C: (A) 0
191 g, (B) 0.5 g, (C) 1.0 g, and (D) 1.5 g; (E): SEM images of Fe₂O₃ samples adding 1.0g SLS
192 without assistance of ultrasound; (F): High magnification of (C).

193 The morphology of the as-prepared Fe₂O₃ nanoparticles are shown in Fig. 4. The
194 changes in morphology before and after the addition of sodium lignosulfonate are
195 noticeable. The pure sample without surface modification is shown in Fig. 4A. It
196 can be clearly seen that the particle of Fe₂O₃ is bulky compared to the modified
197 Fe₂O₃ samples, and the primary particle size is between 200-500 nm. With the
198 increase of SLS content, the size of the particles of iron oxide decreased rapidly. As

199 shown in the Fig. 4C, the as-prepared Fe_2O_3 samples are composed of fine and
200 uniform particles with the addition of 1.0g SLS. Fig. 4F is a higher magnification of
201 Fig. 4C, the synthesized Fe_2O_3 nanoparticles showed smallest grain size (ca. 20 nm
202 in diameter) and abundant porous nanostructure. Such structure exhibits a
203 high-developed surface area. Interestingly, the grain size is raised to 30 nm when
204 the quantity of SLS increased to 1.5g, as shown in Fig. 4D. Meanwhile, it can be
205 clearly observed that severe agglomeration has occurred between particles, which
206 indicates that an excessive increase in the addition amount of SLS is detrimental to
207 the preparation of Fe_2O_3 . The morphology of the Fe_2O_3 sample added 1.0g SLS to
208 the reaction system without ultrasound was also investigated (Fig. 4E), The results
209 suggest that the growth of Fe_2O_3 is nearly uncontrolled, and the particle size of
210 Fe_2O_3 is even larger than 500 nm. The calcining temperature affects the final
211 quality and performance of the powders, so it is essential to discuss and research
212 the influence of the temperature on the preparation of nanomaterials. The typical
213 SEM image of Fe_2O_3 annealed at 300°C is displayed in Fig. 5A. The heavily
214 agglomerated particles and XRD patterns show that the as-prepared precursor is not
215 successfully transformed to Fe_2O_3 crystal under the lower calcination temperature.
216 It can be observed that the particle size show an increasing trend with increase in
217 temperature, and change from smaller than 30 nm at 400°C (Fig. 4C) to about 60
218 nm at 500°C (Fig. 5B). The results showed that the surfactant and the calcining
219 temperature have great influence on the particle size of Fe_2O_3 .
220



221
222

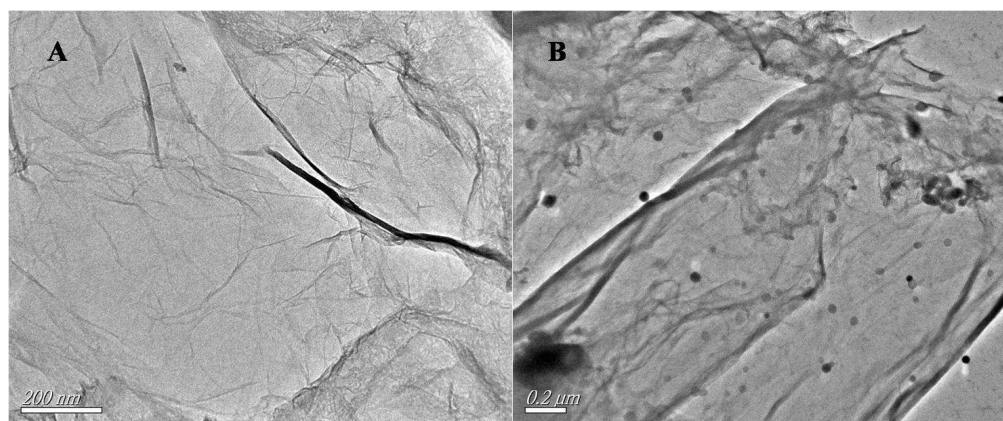
223 Fig. 5 SEM images of Fe_2O_3 samples with the addition of SLS is 1.0 g calcined at 300 °C
224 (A), 500 °C (B).

225 Nitrogen isotherm adsorption-desorption experiment was carried out to examine
226 characteristics of the specific surface areas of the as- prepared Fe_2O_3 under different conditions,
227 the results are shown in Tab.1. Without the addition of SLS, the Fe_2O_3 nanoparticles show small
228 specific surface area of $8.208 \text{ m}^2 \cdot \text{g}^{-1}$. After that, the specific surface areas of the Fe_2O_3 is
229 consistently increasing with the added amount of SLS, and an maximum specific surface areas
230 ($81.319 \text{ m}^2 \cdot \text{g}^{-1}$) was obtained when the SLS is added to 1.0g. The Fe_2O_3 calcined at 400°C
231 display highest specific surface areas than those of 300°C, 500°C and 600°C. By comparing the
232 analysis results of XRD and SEM, We can find that the specific surface areas increases with the
233 decreasing of particle diameter because of the surface effect.

234 According to the SEM, XRD and BET results mentioned above, the impacts of SLS,
235 ultrasonic and calcining temperature on the formation of Fe_2O_3 can be described as follows:
236 First, from the FTIR spectrograms it is observed that sodium lignosulphonate contains a large
237 amount of carboxylic (3437 cm^{-1}) and sulfonic (1044 cm^{-1} and 621 cm^{-1}) groups.^{36,37} After adding
238 the surfactant SLS to ferric chloride solution, SLS produces the negatively-charged sulfonic and
239 carboxylic groups that could form a covalent bond with Fe^{3+} by electrostatic interactions.³⁸ The
240 appropriate SLS concentration leads to the lower Fe^{3+} concentration, which will decrease the
241 nucleation rate of FeOOH . Meanwhile, these negatively charged groups can be absorbed on the

242 crystal nucleus surface under low nucleation rate. These behaviors will help inhibit the crystal
243 nucleus growth and agglomeration. However, when the excessive addition of SLS, these
244 negatively-charged groups might aggregate with other positively-charged groups by
245 electrostatic interactions, and lose its function to suppress the crystal nucleus growth and
246 agglomeration. On the other hand, higher ultrasonic irradiation can generate more nucleation
247 which leads to smaller grain size and more dispersed particles.³⁹ The influence of temperature,
248 we can speculate that the decomposition of FeOOH gradually increased with the increase in
249 calcination temperature, and the high decomposition rate will speed up the crystal growth.
250 Finally, the Fe₂O₃ grain size also continuously increased with the rapid crystal growth rate.

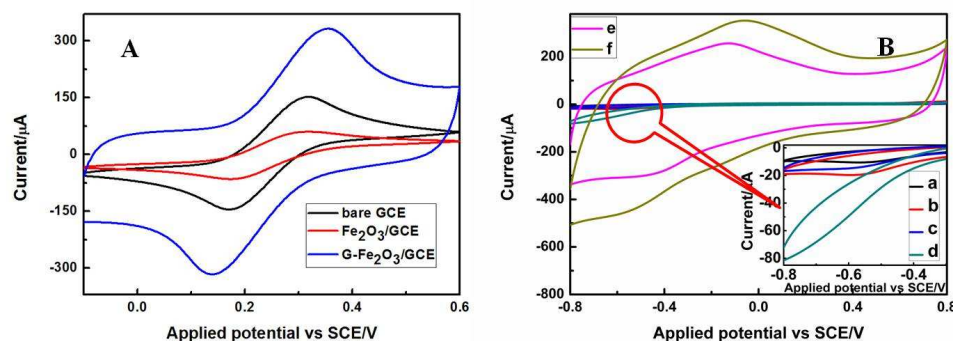
251 TEM images of G and G-Fe₂O₃ shown in Fig. 6 provide strong evidence that Fe₂O₃ has been
252 immobilized on the surface of G by a bridge constituted of chitosan (Black spots or gray dots in
253 Fig.6B). It can be seen from Fig. 6A that the G displays typical semitransparent flakelike and
254 some crumpled shapes, which is attributed to the thin thickness and large surface area of G. This
255 is an advantage for electron transfer on the surface of the electrode. Fe₂O₃ has been tightly
256 stuck to the wrinkled G surface using the chitosan, As shown in Fig. 6B. The average diameter
257 of Fe₂O₃ was estimated to be about 20nm, which is roughly correspondence with the XRD
258 and SEM analysis results.



259
260
261

Fig. 6 TEM images of G (A) and G-Fe₂O₃-NPS-CS (B)

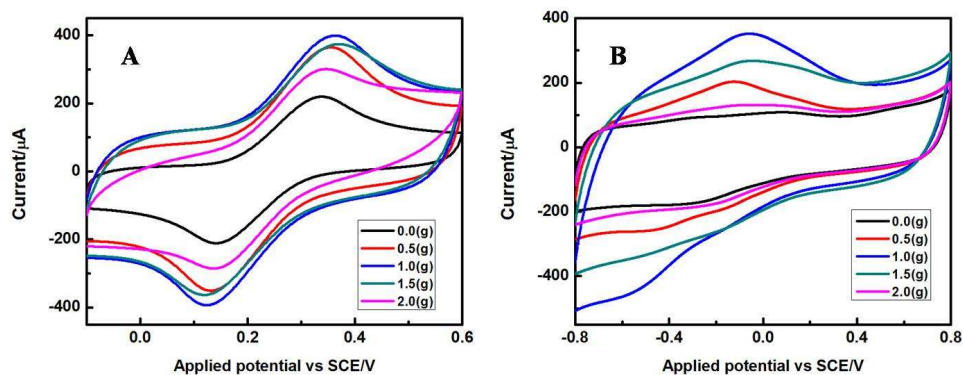
262 The electrochemical properties of the as-prepared Fe_2O_3 nanoparticles modified GCE
263 electrode was detected using cyclic voltammetry in $[\text{Fe}(\text{CN})_6]^{3-/4-}$ solution with the scan rate 50
264 $\text{mV}\cdot\text{s}^{-1}$ at room temperature. First the bare GCE, Fe_2O_3 -NPS-CS/GCE, G- Fe_2O_3 -NPS-CS/GCE
265 electrodes were tested in a solution of 5mM $[\text{Fe}(\text{CN})_6]^{4-/3-}$ containing 0.1M KCl in the range
266 from -0.1 to 0.6 V, as shown in Fig. 7A. Only the Fe_2O_3 modified GCE electrode shows a low
267 pair of redox peaks compared with bare GCE electrode. This could be due to iron oxide
268 semiconductor hinder the electronic transmission on the surface of GCE. In order to improve
269 electrode properties, graphene was introduced into Fe_2O_3 modified GCE. It is clear that the
270 introduction of graphene gives rise to a sharp increase of the peak current. The cyclic
271 voltammogram of the above three electrodes in 0.1M PBS of pH 7.4 in the range from -0.8 to
272 0.8 V with the presence and the absence of 5 mM hydrogen peroxide was shown in Fig. 7B.



273 Fig. 7 (A) CVs of the bare GCE, Fe_2O_3 -NPS -CS/GCE and G- Fe_2O_3 -NPS -CS/GCE in 5mM
274 $[\text{Fe}(\text{CN})_6]^{3-/4-}$ solution (1:1, molar ratio) with 0.1 M KCl. (B) CVs of bare GCE (a and b),
275 Fe_2O_3 -NPS -CS/GCE (c and d) and G- Fe_2O_3 -NPS -CS/GCE (e and f) in the absence (a, c and e)
276 and presence (b, d and f) of 5mM H_2O_2 in 0.1M PBS. Inset: Local amplification of the selected
277 area.
278

279 At the bare electrode in the absence (curve a) and presence (curve b) of H_2O_2 , no obvious
280 current responses were observed. The Fe_2O_3 modified electrode showed an obvious current
281 response at about -0.38V in the presence of H_2O_2 (curve d). It can clearly be seen that, after
282 adding the graphene into the modified electrode (G- Fe_2O_3 -NPS-CS/GCE), the current response
283 of the electrode dramatically increases. The results display that the electron transfer rate of the

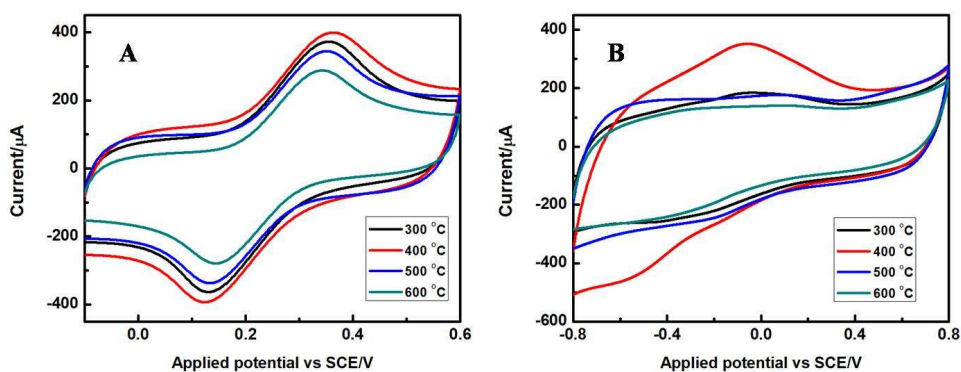
284 G-Fe₂O₃-NPS-CS/GCE is much higher than that of the Fe₂O₃-NPS-CS/GCE. Meanwhile, the
 285 G-Fe₂O₃-NPS-CS/GCE modified electrode also show excellent sensitivity to H₂O₂ (curve f),
 286 which could be attributed to electrochemical signal amplification through the good conductivity
 287 and the large surface area of the graphene. It also indicated that the G-Fe₂O₃-NPS-CS/GCE
 288 composite sensor was developed successfully.
 289



290
 291 Fig.8 CVs of G-Fe₂O₃-NPS-CS/GCE in 5mM [Fe(CN)₆]^{3-/4-} solution (1:1, molar ratio) with
 292 0.1 M KCl (A) and in 0.1M PBS (pH=7.4) containing 5mM H₂O₂ (B), the Fe₂O₃-NPS used in
 293 this experiment were calcined at 400°C, and with the addition of 0g, 0.5g, 1.0g, 1.5g, and 2.0g
 294 SLS .
 295

296 The electrochemical properties of the as-prepared Fe₂O₃ nanoparticles with different addition
 297 amount of SLS calcined under 400°C are shown in Fig. 8. Fig. 8A depicts the cyclic
 298 voltammogram of these modified electrodes in 5mM [Fe(CN)₆]^{4-/3-} containing 0.1M KCl, it is
 299 found that all electrodes exhibited a pair of obvious redox peaks, and the current response
 300 gradually increased with the addition of SLS. The value of redox peak current reached the
 301 maximum at the addition of 1.0g SLS. However, the redox peak current was accompanied by a
 302 dramatical decrease with a further increase of SLS. Fig 8B shows the CVs of the Fe₂O₃
 303 modified electrode in 0.1M PBS (pH 7.4) toward the reduction of 5mM H₂O₂. A similar
 304 phenomenon in which the current response increased with the addition of SLS was observed for
 305 these electrodes. After added 1.0g, the sensitivity of the sensor to hydrogen peroxide started to

306 decline gradually with the continuous addition of SLS. Therefore, we can come to the
307 conclusion that it is detrimental for preparation of sensor due to an excessive addition of SLS.

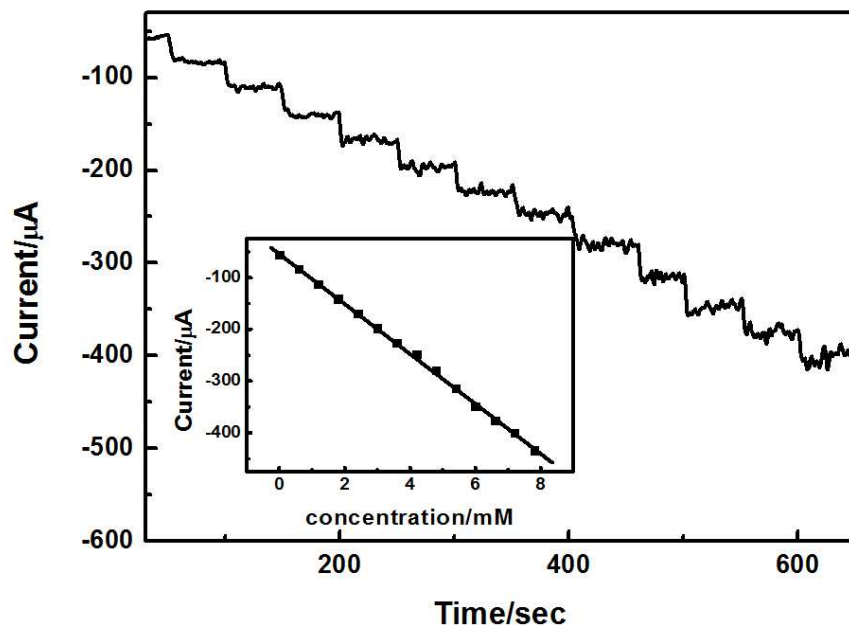


308
309 Fig. 9 CVs of G-Fe₂O₃-NPS -CS/GCE in 5mM [Fe(CN)₆]^{3-/4-} solution (1:1, molar ratio)
310 with 0.1 M KCl (A) and in 0.1M PBS (pH=7.4) with 5 mM H₂O₂ (B), the Fe₂O₃-NPS used
311 in this experiment were doped with 1.0 g SLS, and caicined at 300 °C, 400 °C, 500 °C and
312 600 °C.

313

314 Fig. 9 shows the cyclic voltammograms of different G/Fe₂O₃-NPS/CS/CPEs in which the
315 Fe₂O₃-NPS calcined at various temperatures. The electron transfer rate between the G-Fe₂O₃
316 composite film and electrode surface was studied in 5mM [Fe(CN)₆]^{4-/3-} containing 0.1M KCl,
317 as shown in Fig. 9A. When the Fe₂O₃ was calcined at 400°C, the electron transfer rate of the
318 G/Fe₂O₃-NPS/CS/CPE is faster than that of the others. Electrochemical properties of the
319 as-prepared modified electrodes are further detected in the presence of 5mM H₂O₂ in 0.1M PBS
320 (pH=7.4). It can be seen from Fig. 9B that the current response of the G/Fe₂O₃-NPS/CS/CPE
321 modified electrode (Fe₂O₃ calcined at 400°C) at the -0.38v was improved 10%, 20% and 30%
322 respectively, compared with other three electrodes (Fe₂O₃ calcined at 300°C, 500°C and 600°C).
323 Apparently, The above presented results indicated that calcination temperature is an important
324 influencing factor during the preparation process of Fe₂O₃. Combining with the analyses of
325 XRD, SEM and CVs, it can be found that the sensitivity of the H₂O₂ sensor increases with
326 decreasing of Fe₂O₃ nanoparticle size. We speculate that this may be due to the intense surface

327 force field, lack of particle coordination and elevated defects of the small particles with larger
328 specific surface area, which are beneficial to the absorbance of H_2O_2 in solution .



329 Fig. 10. Amperometric response of sensor to H_2O_2 concentration in 0.1M pH=7.4 PBS at
330 -0.38 V. Inset: linear plot
331
332

333 Finally, the sensitivity of G- Fe_2O_3 -CS/GCE-1-400 is estimated by chronoamperometry
334 measuring the current response with the gradually addition of H_2O_2 to 0.1M BPS of pH 7.4 at
335 fixed potential of -0.38 V. As shown in the Fig. 10 the sensor showed a fast amperometric
336 response time less than 2s, which is greatly shortened compared to the previous literature
337 reported for other H_2O_2 sensors.^{13,40,41} Meanwhile, with the increasing of H_2O_2 concentration,
338 the amperometric response of the G- Fe_2O_3 -CS/GCE-1-400 electrode increased linearly (Tab. 2).
339 The linear regression equation was expressed as: $I_p(\text{A}) = -53.02 - 48.43 [\text{H}_2\text{O}_2](\text{mM})$ in the
340 wide calibration range from 0.5 to 7800 μM with a correlation coefficient of 0.999. A low
341 detection limit of 0.5 μM is estimated at the signal to noise of 3. The sensitivity of the
342 G- Fe_2O_3 -CS/GCE-1-400 electrode is calculated to be 385.59 ($\mu\text{A mM}^{-1} \text{cm}^{-2}$) by the slope of

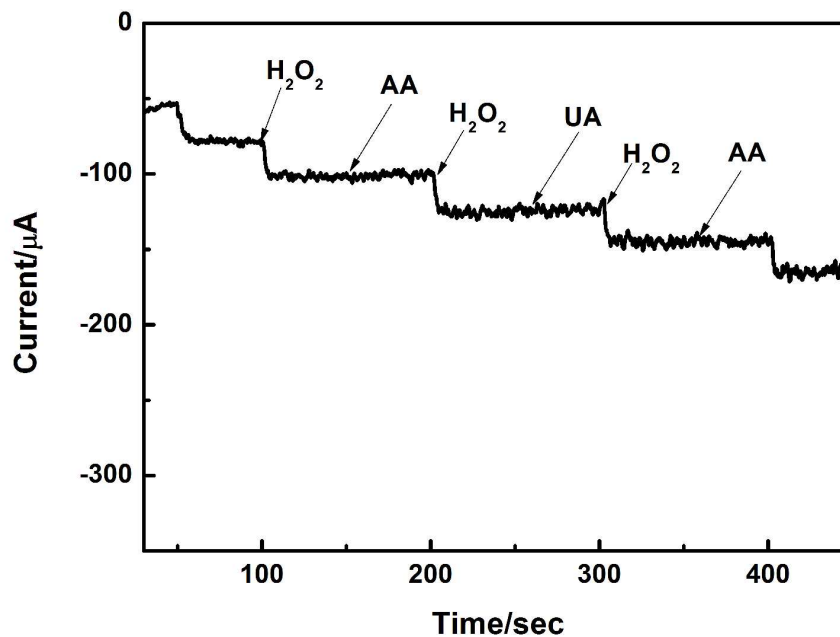
343 the linear regression curve. The as-prepared electrode exhibits high sensitivity and a low
344 detection limit compared to other modified electrodes, such as the Ag-nanobrous
345 membrane/GCE⁶, heme protein-SWCNT-CTAB electrodes⁴² and CTAB-SAMN/CPE⁴³. These
346 results demonstrate that H₂O₂ could be easily detected used as-prepared modified electrode.

347 Anti-interference test, being the crucial influence factor, can never be neglected in the
348 determination of any objects by electrochemical method. Therefore, the influence of common
349 interfering substances such as ascorbic (AA) and uric acid (UA) was studied by amperometric
350 method. The results is shown in the Fig.11, the modified electrode show a weak current
351 response to the addition of 5mM AA and UA with the 0.1M BPS of pH 7.4 at fixed potential of
352 -0.38 V. This illustrates the proposed sensor well prevented the influence of interfering
353 substances. Stability and repeatability studies were conducted to further detection the
354 electrochemical performance of G-Fe₂O₃-CS/GCE-1-400 sensor. The stability is evaluated by
355 testing the average current response of the modified electrode after prepared 1 day, 1 week, 1
356 month and 2 month and the biosensor retained over 90% response of its initial sensitivity to the
357 reduction of H₂O₂, demonstrating its good long-term stability. Cyclic Voltammetry experiments
358 were repeatedly performed for 15 times with the G-Fe₂O₃-CS/GCE-1-400 sensor in the
359 presence of H₂O₂. The relative standard deviation was approximately 1.89%, which indicated
360 that the reproducibility of as-prepared sensor was excellent.

361 Tab. 2 Comparison of the linear range (LR), sensitivity, detection limit (DL) and response
362 time (RT) of hydrogen peroxide sensors

Electrode materials	LR (μM)	Sensitivity	DL (μM)	RT	Reference
Ag-nanobrous membrane/GCE	10-16500	$157 \mu\text{A mM}^{-1} \text{cm}^{-2}$	4		6
Au/graphene/HRP/CS/GCE	5.0-5130		1.7	< 3S	13
AgNPs/Ox-pTTBA/MWCNT	10-260		0.24	< 5S	40
Hb/HMS-modified GCEs	0.4-6.0		1.86×10^{-3}	< 5S	41
$\alpha\text{-Fe}_2\text{O}_3$ NR arrays	0.2-5000	$135.36 \mu\text{A mM}^{-1} \text{cm}^{-2}$	0.1		42
CTAB-SAMN/CPE	10-1500	$58 \mu\text{A mM}^{-1} \text{cm}^{-2}$	2.78		43
G- Fe_2O_3 -NPS-CS/GCE	0.5- 7800	$385.59 \mu\text{A mM}^{-1} \text{cm}^{-2}$	0.5	< 2S	This work

363



364

365 Fig. 11. Amperometric response of sensor to 5mM H₂O₂, AA and UA in 0.1M pH=7.4 PBS at
366 -0.38 V.

367

368 Conclusion

369 In summary, a convenient, economic method for preparing a Fe₂O₃ nanoparticles using SLS
370 as a surfactant by liquid phase-based ultrasonic-assisted method was proposed in this paper. The
371 as-prepared Fe₂O₃ nanoparticles show a small and homogeneous size distribution with a high
372 specific surface area when the addition amount of SLS in the synthetic system was 1g, and the
373 α-FeOOH precursor was calcined at 400°C. The G-Fe₂O₃-CS/GCE-1-400 modified electrode
374 showed highest electrocatalytic activity toward the detection of H₂O₂. Chronoamperometry
375 measuring revealed that the prepared sensor exhibits high sensitivity, low detection limit, wide
376 linear range, fast response time, good stability and anti-interference ability. Hence, the
377 as-prepared G-Fe₂O₃-CS/GCE modified electrode provides an effective way for the preparation
378 of the high-performance enzyme-free sensor.

379

380 **Acknowledgment**

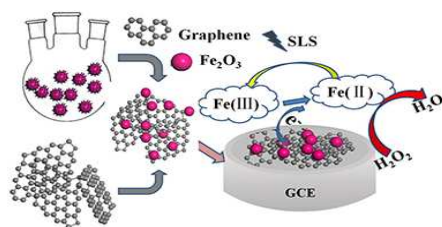
381 We gratefully acknowledge the National Natural Science Foundation of China (21375050,
382 61171015), the Open Project Program of State Key Laboratory of Analytical Chemistry for
383 Life Science (Nanjing University) (KLACLS1010), the Program of Department of Education of
384 Jiangsu Province (12KJD610003), and the Natural Science Foundation of Jiangsu Province
385 (BK20131249) for financial support of this research.

386 **References**

- 387 [1] B. H. Kim, M J. Hackett, J. Park, and T Hyeon, *Chem. Mater.*, 2014, 26, 59-71.
388
389 [2] X. S. Liu, N. Huang, H. Li, Q. Jin, and J. Ji, *Langmuir*, 2013, 29, 9138-9148.
390
391 [3] J. S. Son, J. S. Lee, E. V. Shevchenko, and D. V. Talapin, *J. Phys. Chem. Lett.*, 2013, 4,
392 1918-1923.
393
394 [4] Y. D. Yin, and D. Talapin, *Chem. Soc. Rev.*, 2013, 42, 2484-2487.
395
396 [5] N. Iqbal, A. Afzal, and A. Mujahid, *RSC Adv.*, 2014, 4, 43121-43130.
397
398 [6] D. W. Li, L. Luo, Z. Y. Pang, X. D. Chen, Y. B. Cai and Q. F. Wei, *RSC Adv.*, 2014, 4,
399 3857-3863.
400
401 [7] A. Sarkar, A. K. Singh, G. G. Khan, D. Sarkar, and K. Mandal, *RSC Adv.*, 2014, 4,
402 55629-55634.
403
404 [8] J. Lyytinen, M. Berdova, P. Hirvonen, X. W. Liu, S. Franssila, Q. Zhou, and J. Koskinen,
405 *RSC Adv.*, 2014, 4, 37320-37328.
406
407 [9] X. H. Wang, Y. K. Zhang, C. Hao, F. Feng, H. B. Yin, and N. C. Si, *Ind. Eng. Chem. Res.*,
408 2014, 53, 6585–6592.
409
410 [10] H. Y. Zhao, W. Zheng, Z. X. Meng, H. M. Zhou, X. X. Xu, Z. Li, Y. F. Zheng, *Biosens.*
411 *Bioelectron.*, 2009, 24, 2352–2357.
412
413 [11] Z. L. Liu, K. X. Wang, L. Xiao, X. J. Chen, X. D. Ren, J. T. Lu, and L. Zhuang, *RSC Adv.*,
414 2014, 4, 37701-37704.
415
416 [12] S. H. Chen, R. Yuan, Y. Q. Chai, L. G. Zhang, N. Wang, X. L. Li, *Biosens. Bioelectron.*,
417 2007, 22 , 1268-1274.

- 418
419 [13] K. F. Zhou, Y. H. Zhu, X. L. Yang, J. Luo, C. Z. Li, S. R. Luan, *Electrochim. Acta*, 2010,
420 55, 3055-3060.
421
422 [14] K. J. Huang, D. J. Niu, X. Liu, Z. W. Wu, Y. Fan, Y. F. Chang, Y. Y. Wu, *Electrochim. Acta*,
423 2011, 56, 2947-2953.
424
425 [15] M. G. Li, S. D. Xu, M. Tang, L. Liu, F. Gao, Y. L. Wang, *Electrochim. Acta*, 2011,
426 56, 1144-1149.
427
428 [16] Z. F. Wang, F. Liao, T. T. Guo, S. W. Yang, C. M. Zeng, *J. Electroanal. Chem.*, 2012, 664,
429 135-138.
430
431 [17] T. S. Liu, T. F. Kang, L. P. Lu, Y. Zhang, S. Y. Cheng, *J. Electroanal. Chem.*, 2009, 632,
432 197-200.
433
434 [18] S. H. Chen, R. Yuan, Y. Q. Chai, L. Y. Zhang, N. Wang, X. L. Li, *Biosens. Bioelectron.*,
435 2007, 22, 1268-1274.
436
437 [19] M. Shamsipura, M. Asgari, M. G. Maragheh, A. A. Moosavi-Movahedi,
438 *Bioelectrochemistry*, 2012, 83, 31-37.
439
440 [20] J. Hong, W. Y. Yang, Y. X. Zhao, B. L. Xiao, Y. F. Gao, T. Yang, H. Ghourchian, Z.
441 Moosavi-Movahedi, N. Sheibani, J. G. Li, A. A. Moosavi-Movahedi, *Electrochim. Acta*, 2013,
442 89, 317-325.
443
444 [21] L. Aghebati-maleki, B. Salehi, R. Behfar, H. Saeidmanesh, F. Ahmadian, M.
445 Sarebanhassanabadi, and M. Negahdary, *Int. J. Electrochem. Sci.*, 2014, 9, 257 - 271.
446
447 [22] M. Shamsipur, M. Asgari, M. F. Mousavi, R. Davarkhah, *Electroanaly.*, 2012, 24, 357-367.
448
449 [23] A. T. Ezhil Vilian, and S. M. Chen, *RSC Adv.*, 2014, 4, 55867-55876.
450
451 [24] B. B. Jiang, X. W. Wei, F. H. Wu, K. L. Wu, L. Chen, G. Z. Yuan, C. Dong, Y. Ye,
452 *Microchim. Acta*, 2014, 181, 1463-1470.
453
454 [25] L. M. Li, Z. F. Du, S. Liu, Q. Y. Hao, Y. G. Wang, Q. H. Li, T. H. Wang, *Talanta*, 2010, 82,
455 1637-1641.
456
457 [26] A. P. Liu, W. J. Dong, E. J. Liu, W. H. Tang, J. Q. Zhu, and Ji. C. Han, *Electrochim. Acta*,
458 2010, 55, 1971-1977.
459
460 [27] Z. Y. Miao, D. Zhang, and Q. Chen, *Materials*, 2014, 7, 2945-2955.
461
462 [28] H. Y. Sun, H. Q. Yuan, Z. M. Liu, B. X. Han, and X. R. Zhang, *Adv. Mater.*, 2005, 17,
463 2993-2997.
464

- 465 [29] M. Y. Zhu, Y. Wang, D. H. Meng, X. Z. Qin, and G. W. Diao, *J. Phys. Chem. C*, 2012, 116,
466 16276-16285.
467
- 468 [30] S. W. Cao, and Y. J. Zhu, *J. Phys. Chem. C* 2008, 112, 6253-6257.
469
- 470 [31] Q. Zhang, X. w. Lu, L. Y. Chen, Y. X. Shi, T. Xu, M. L. Liu, *Mater. Lett.*, 2013, 106,
471 447–451.
472
- 473 [32] X. M. Liu, S. Y. Fu, H. M. Xiao, C. J. Huang, *J. Solid State Chem.*, 2005, 178,
474 2798-2803.
475
- 476 [33] S. Bai, X. P. Shen, X. Zhong, Y. Liu, G. X. Zhu, X. Xu, K. M. Chen, *Carbon*, 2012, 50,
477 2337-2346.
478
- 479 [34] X. H. Liao, J. J. Zhu, W. Zhong, H. Y. Chen, *Mater. Lett.*, 2001, 50, 341-346.
480
- 481 [35] B. Zhao, Y. Wang, H. Guo, J. Wang, Y. He, Z. Jiao, M. Wu, *Mater. Sci.-Poland*, 2007, 25,
482 1143-1148.
483
- 484 [36] G. Yu, B. Li, H. S. Wang, C. Liu, and X. D. Mu, *BioResources*, 2013, 8, 1055-1063.
485
- 486 [37] D. Ji, Z. Y. Luo, M. He, Y. J. Shi, X. L. Gu, *Cement Concrete Res.*, 2012, 42, 1199-1206.
487
- 488 [38] T. T. Miao, Y. R. Guo, Q. J. Pan, *J. Nanopart Res.*, 2013, 15, 1725-1737.
489
- 490 [39] S. Allahyari, M. Haghghi, A. Ebadi, S. Hosseinzadeh, *Ultrason. Sonochem.*, 2014, 21,
491 663-673.
492
- 493 [40] A. Abdelwahab, Y-B. Shim, *Sensor. Actuat. B-Chem.*, 2014, 201, 51-58.
494
- 495 [41] Z. H. Dai, S. Q. Liu, H. X. Ju, H. Y. Chen, *Biosens. Bioelectron.*, 2004, 19, 861-867.
496
- 497 [42] X. J. Liu, J. F. Liu, Z. Chang, L. Luo, X. D. Lei, X. M. Sun, *RSC Adv.*, 2013, 3, 8489-8494.
498
- 499 [43] M. Magroa, D. Baratella, N. Pianca, A. Toninello, S. Grancarab, R. Zboril, F. Vianello,
500 *Sensor. Actuat. B-Chem.*, 2013, 176, 315-322.



The as-prepared G-Fe₂O₃-NPS-CS/GCE sensor using the synthesized Fe₂O₃ under the ultrasonic-assisted method displayed an excellent electrochemical activity for hydrogen peroxide.